

Determining Young's and shear moduli of a rod-shaped object in an AFM bending test

Alexander V. Ankudinov^{1,a}, Mikhail S. Dunaevskiy^{1,b}, Andrei A. Krasilin^{1,c},
Maksim M. Khalisov^{1,2,d}, Ekaterina K. Khrapova^{1,e}

¹Ioffe Institute, St. Petersburg, Russia

²Pavlov Institute of Physiology, Russian Academy of Sciences, St. Petersburg, Russia

^aalexander.ankudinov@mail.ioffe.ru, ^bmike.dunaeffsky@mail.ioffe.ru, ^cikrasilin@mail.ioffe.ru,

^dkhalisovmm@infran.ru, ^earganella@yandex.ru

Corresponding author: A. V. Ankudinov, alexander.ankudinov@mail.ioffe.ru

PACS 07.79.Lh, 62.20.F, 81.70.Bt

ABSTRACT The technique of AFM bending test of a suspended nanoobject has been improved. An analytical method has been created for calculating Young's and shear moduli of object's material based on data of such tests. In Timoshenko approximation, we consider problems of bending a beam one or both ends of which lie on elastic Winkler foundations. The obtained solutions are used to eliminate uncertainties in the calculation of elastic moduli that arise when the conditions of fixing an object (console or bridge) on the edges of a recess in the substrate are unknown.

KEYWORDS atomic force microscopy, bending, nanoscroll, elastic moduli, elastic Winkler foundation.

ACKNOWLEDGEMENTS This work was supported by the Russian Science Foundation, project no. 19-13-00151.

FOR CITATION Ankudinov A.V., Dunaevskiy M.S., Krasilin A.A., Khalisov M.M., Khrapova E.K. Determining Young's and shear moduli of a rod-shaped object in an AFM bending test. *Nanosystems: Phys. Chem. Math.*, 2024, **15** (1), 122–129.

1. Introduction

Atomic force microscopy (AFM) [1,2] is effectively used for bending tests [3–6] of suspended rod-shaped nanoobjects (consoles, bridges). According to the theory of elasticity for slight bending of rods in the Euler–Bernoulli approximation [7], based on the stiffness or deformation profiles measured using AFM and the dimensions of the suspended part of the object, one can calculate the Young's modulus E of the object. First of all, it is important to exclude possible errors in AFM measurements of contact stiffness associated with the characteristics of the tip–sample contact (whether the tip slides along the surface or is clamped), the sample topography, and other factors, see [8]. Then, for correct calculation, it is necessary to know the conditions for fixing the object to recess edges. This information can be obtained by comparing test data with model bending profiles [9–15]. In paper [15], analytical dependence was obtained for the bending profiles of model beams (consoles and bridges), supported, in particular, on elastic Winkler foundations [16].

To apply the Euler–Bernoulli approximation, it is required that the shear displacements w_S be much less than the bending displacements w_B . In an isotropic elastic material, $G/E \geq 1/3$ (the shear modulus $G = E/(2[1 + \nu])$, Poisson's ratio $\nu \in [-1, 0.5]$). Therefore, in a thin rod (with the transverse diameter d much smaller than the length l), this requirement is satisfied, $w_S/w_B \sim d^2/l^2 \ll 1$. It is also believed [17] that for an anisotropic crystalline material in this approximation the Young's modulus E is determined along the long axis of the rod-shaped object. However, from the theoretical point of view [18], there is no limit for the value of ν for an anisotropic material, and G/E can be so small that $w_S \sim w_B$. This necessitates allowance for shear strains in AFM bending test of a rod-shaped object.

In this paper, the problems of bending of model consoles and bridges are solved taking into account shear strains in the Timoshenko approximation [19]. As before [15], three types of conditions for fixing the ends of the beam were studied, Fig. 1: clamping, ring spring, and elastic Winkler foundation. The analytical dependence obtained for the bending profiles of consoles and bridges was used to process the data from AFM bending tests of $\text{MgNi}_2\text{Si}_2\text{O}_5(\text{OH})_4$ nanoscrolls [15].

2. Calculation results

Figure 2 shows diagrams of shear only (a) and bending only (b) of a console loaded with a vertical force. In Fig. 2a, only tangential mechanical stresses τ_{xz} act in the console section with area A . They are parallel to the force $\mathbf{F} = F_z$ and balance it in any such console section. The console displacement w_S is proportional to the distance x to the pinch point and inversely proportional to G ,

$$w_S = \theta x, \quad F_z = A\tau = AG\theta, \quad w_S = [F_z/GA]x, \quad (1)$$

where θ is the angle. Strictly speaking, τ_{xz} is distributed nonuniformly over the beam section. This can be taken into account by adjusting the shear modulus $G = \kappa G$ using the Timoshenko shear coefficient κ , $\kappa = 6(1 + \nu)/(7 + 6\nu) \approx 1$ for a cylindrical rod [19, 20].

In Fig. 2b, only normal mechanical stresses σ_{xx} act in the console section at point x . They are perpendicular to F_z and balance the moment of force $F_z(l - x)$. The console displacements w_B obey the differential equation

$$d^2 w_B / dx^2 \cong 1/R(x) = [F_z(1 - \nu^2)/EI](l - x), \quad (2)$$

where I is the moment of inertia of the beam section ($I = \pi d^4/64$ for a circular section with diameter d). Usually ν is small (≈ 0.25), and the factor $(1 - \nu^2)$ is close to unity and may not be presented in the formula for solving Eq. (2) [7],

$$w_B = [F_z/6EI]x^2(3l - x). \quad (2a)$$

The resulting console displacement is $w = w_B + w_S$. In AFM, the displacement of a suspended object can only be measured at the point where the force is applied. The theoretical dependence for such a displacement is obtained by using the substitution $l = x$ in the formula for w_B ,

$$w = [F_z/3EI]x^3 + [F_z/GA]x. \quad (3)$$

To interpret AFM data, it is convenient to use the normalized displacement profile $\zeta(\chi) = w/w_{MAX}$, depending on the dimensionless variable $\chi = x/l$,

$$\zeta_{C1}(\chi) = (\chi^3 + 3\gamma\chi)/(1 + 3\gamma), \quad (4)$$

for the following fitting parameter $\gamma = [EI/GAl^2]$.

Let us write expression (3) in two equivalent ways:

$$w = [F_z l^3/3EI](\chi^3 + 3\gamma\chi), \quad (3a)$$

$$w = [F_z l/GA](\chi + \chi^3/3\gamma). \quad (3b)$$

If $\gamma = 0$, then only the cubic dependence of the bending on x remains in (3a). If $\gamma \rightarrow \infty$, only the linear dependence of the shear on x is left in (3b). Assuming that the experiment satisfies one of these limiting extremes, we can calculate only E or only G of the console, which below are referred to as the zero versions of elastic moduli or their values according to the zero model,

$$\begin{aligned} E_{C0} &= [F_z l^3/3w_{MAX}I] = [l^3/3I]k_C, \\ G_{C0} &= [l/A]k_C, \end{aligned} \quad (5)$$

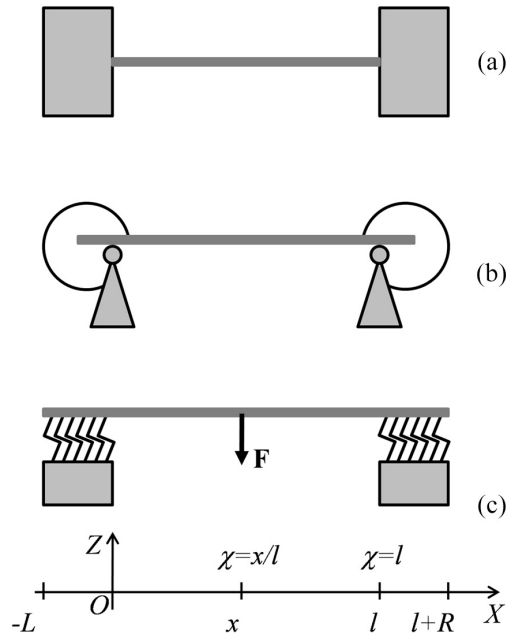


FIG. 1. Options for fixing conditions. Clamping: (a), model 1. Ring spring: (b), model 2. Elastic Winkler foundation (Winkler coefficient k_W , lengths L and R , origin on the left support, bridge length l , force F applied at point x): (c), model 3.

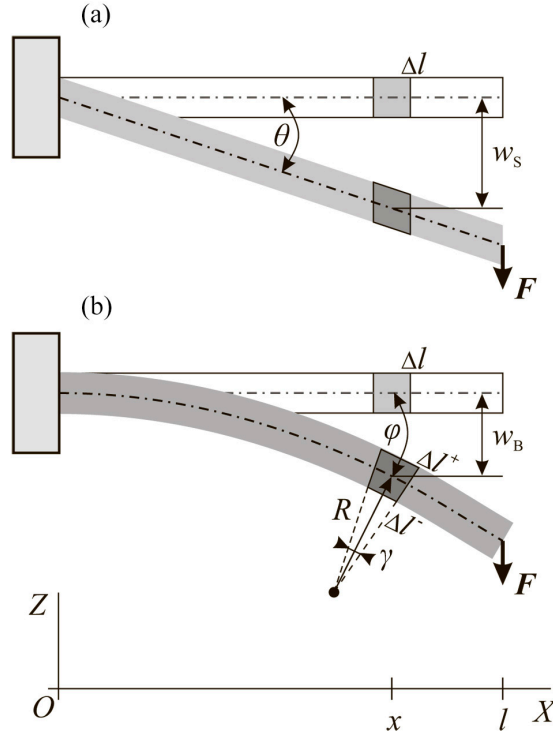


FIG. 2. Shear only (a) and bending only (b) of a console of length l and thickness t . The force $\mathbf{F} = F_z$ transforms a rectangular section of length Δl into a parallelepiped with vertex angles $\pi/(2 \pm \theta)$ (a) and into an isosceles trapezoid with bases stretched to Δl^+ and compressed to Δl^- and an angle between the sides $\gamma = (\Delta l^+ - \Delta l^-)/t$, corresponding to the local curvature radius $R = \Delta l/\gamma$ (b).

where k_C is the minimum console stiffness. For a bridge with minimum stiffness k_B , the formulas for calculating the zero versions of elastic moduli are as follows:

$$\begin{aligned} E_{B0} &= [l^3/192I]k_B, \\ G_{B0} &= [l/4A]k_B. \end{aligned} \quad (5a)$$

Based on the value of γ that matches the fitting dependences (3) and (4) with the experimental bending profile, both elastic moduli can be determined in intermediate cases,

$$\begin{cases} E_1 = \Phi_{EC1}E_{C0}, & \Phi_{EC1} = 1 + 3\gamma, \\ G_1 = \Phi_{GC1}G_{C0}, & \Phi_{GC1} = 1 + (3\gamma)^{-1} = \Phi_{EC1}(3\gamma)^{-1}, \end{cases} \quad (6)$$

where we have introduced Φ_{EC1} and Φ_{GC1} — correction factors according to model 1, Fig. 1.

Relations similar to (4) and (6) can also be derived for models 2 and 3 of boundary conditions, Fig. 1. The displacements of the suspended beam span in the Timoshenko approximation satisfy the equations

$$\begin{cases} d^3\varphi/dx^3 = 0, \\ dw/dx = \varphi - [EI/GA]d^2\varphi/dx^2. \end{cases} \quad (7)$$

In this approximation, the displacements of a beam segment on an elastic foundation obey the equations

$$\begin{cases} d^4\varphi/dx^4 - [k_W/GA]d^2\varphi/dx^2 + [k_W/EI]\varphi = 0, \\ w = -[EI/k_W]d^3\varphi/dx^3. \end{cases} \quad (8)$$

When a rigid cylinder is pressed into a softer elastic base with Young's modulus E_B , the Winkler coefficient in (8) is estimated to be $k_W \approx E_B$ [15].

General solutions to systems (7) and (8) are, respectively, $w = \sum_{k=0}^3 a_k x^k$ and $w = A_0 \exp(\beta_1 x) + A_1 \exp(-\beta_1 x) + A_2 \exp(\beta_2 x) + A_4 \exp(-\beta_2 x)$. The exponents β_1 and β_2 are related by $\beta_1^2 + \beta_2^2 = [k_W/GA]$ and $\beta_1^2 \beta_2^2 = [k_W/EI]$. If $[k_W EI/4G^2 A^2] < 1$, then β_1 and β_2 are a pair of complex conjugate numbers, otherwise positive real numbers. The unknowns a_k and A_k are found from the boundary conditions (see Table 1). As a result, for a bridge and console in each case of fixing conditions in Fig. 1, we obtained simultaneous systems of linear equations, which were solved analytically,

see, for example, the paper [15]. To speed up the calculations, we used computer algebra programs `Mathematica` (Wolfram Research, USA) and `Mathcad` (PTC, USA).

Tables 2 and 3 list the final fitting relationships and correction factors for a console and bridge in the cases of clamped ends and ends supported on ring springs (Fig. 1). More cumbersome solutions for the model with an elastic Winkler foundation are discussed separately below.

For a cantilever beam (a suspended segment of length l , a segment on an elastic foundation of length L), the following exact fitting relationship was obtained:

$$\zeta_{C3}(\chi) = \sum_0^3 c_k \beta_l^k \chi^k / \sum_0^3 c_k \beta_l^k. \quad (9)$$

$$\begin{aligned} c_0 &= 6 \sin(\theta) \left[\sin(\theta/2) \sinh(2\lambda\beta_l \cos(\theta/2)) - \cos(\theta/2) \sin(2\lambda\beta_l \sin(\theta/2)) \right], \\ c_1 &= 6 \sin^2(\theta) \left[\cosh(2\lambda\beta_l \cos(\theta/2)) - \cos(2\lambda\beta_l \sin(\theta/2)) \right], \\ c_2 &= 6 \sin(\theta) \left[\sin(\theta/2) \sinh(2\lambda\beta_l \cos(\theta/2)) + \cos(\theta/2) \sin(2\lambda\beta_l \sin(\theta/2)) \right], \\ c_3 &= 2 \left[\sin^2(\theta/2) \cosh(2\lambda\beta_l \cos(\theta/2)) + \cos^2(\theta/2) \cos(2\lambda\beta_l \sin(\theta/2)) - 1 \right]. \end{aligned}$$

The factors for correction of elastic moduli corresponding to (9) are

$$\begin{aligned} \Phi_{EC3} &= \sum_0^3 c_k \beta_l^k / 2D, \\ \Phi_{GC3} &= [\beta_l^2 / 6 \cos \theta] \Phi_{EC3}; \\ D &= \beta_l^3 \left[1 - \sin^2(\theta/2) \cosh(2\lambda\beta_l \cos(\theta/2)) - \cos^2(\theta/2) \cos(2\lambda\beta_l \sin(\theta/2)) \right]. \end{aligned} \quad (10)$$

TABLE 1. Versions of boundary conditions

Boundary	Conditions
Clamping	$w = \varphi = 0$
Foundation	$w = d\varphi/dx = 0$
Ring spring	$w = 0, d\varphi/dx = [4/\lambda l]\varphi$
Free end	$d\varphi/dx = d^2\varphi/dx^2 = 0$
Point of load F on console	$d\varphi/dx = 0,$ $d^2\varphi/dx^2 = -[F/EI]$
Point of load F on bridge	$w_+ - w_- = \varphi_+ - \varphi_- = 0,$ $d(\varphi_+ - \varphi_-)/dx = 0,$ $d^2(\varphi_+ - \varphi_-)/dx^2 = [F/EI]$

TABLE 2. Calculation of elastic moduli of console in Timoshenko approximation ($\lambda, \gamma \in [0, \infty)$, $\chi \in [0, 1]$. $E_j = \Phi_{ECj} E_{C0}$, $G_j = \Phi_{GCj} (3\gamma)^{-1} G_{C0}$. $E_{C0} = 64[l^3/3\pi d^4]k_C$, $G_{C0} = 4[l/\pi d^2]k_C$).

j , model no.	ζ_{Cj}	Φ_{ECj}
1	$\frac{\chi^3 + 3\gamma\chi}{1 + 3\gamma}$	$1 + 3\gamma$
2	$\frac{\chi^3 + 3\lambda\chi^2 + 3\gamma\chi}{1 + 3\lambda + 3\gamma}$	$1 + 3(\lambda + \gamma)$

TABLE 3. Calculation of elastic moduli of bridge in Timoshenko approximation ($\lambda, \gamma \in [0, \infty)$, $\chi \in [0, 1]$. $E_j = \Phi_{EBj} E_{B0}$, $G_j = \Phi_{EBj} (3\gamma)^{-1} G_{B0}$. $E_{B0} = [l^3/3\pi d^4] k_B$, $G_{B0} = 4[l/\pi d^2] k_B$).

j , model no.	ζ_{Bj}	Φ_{EBj}
1	$64 \left\{ \frac{(\chi - \chi^2)^3 + 3\gamma(\chi - \chi^2)^2}{(1 + 12\gamma)(1 + 48\gamma)} + \frac{3\gamma(\chi - \chi^2)}{(1 + 48\gamma)} \right\}$	$1 + 48\gamma$
2	$64 \left\{ \frac{(2\lambda + 1)(\chi - \chi^2)^3 + 3[\lambda(4\lambda + 1) + (8\lambda + 1)\gamma](\chi - \chi^2)^2}{(1 + 6\lambda + 12\gamma)(1 + 8\lambda + 48(2\lambda + 1)\gamma)} + \frac{3(2\lambda + 1)\gamma(\chi - \chi^2)}{(1 + 8\lambda + 48(2\lambda + 1)\gamma)} \right\}$	$\frac{1 + 8\lambda}{1 + 2\lambda} + 48\gamma$

The dimensionless parameters in (9) and (10) are: $\lambda = L/l$, measured from AFM topography data, and β_l and θ , determined by fitting. Here are the expressions for the fitting parameters:

$$\begin{aligned} \beta_l &= l \sqrt[4]{k_W/EI}, \\ \cos \theta &= \sqrt{k_W EI/4G^2 A^2}. \end{aligned} \quad (11)$$

In (11), β_l is $\sqrt{2}$ times greater than the parameter designated in the same way in the paper [15]. The Winkler elastic foundation coefficient is calculated as

$$k_W = 2GA\beta_l^2 \cos \theta/l^2.$$

For a bridge with span length l (see Fig. 2), only asymptotic solutions ($L\beta_l/l, R\beta_l/l \gg 1$) turn out to be relatively compact,

$$\zeta_{B3}(\chi) = \sum_0^3 b_k \beta_l^k (\chi - \chi^2)^k / \sum_0^3 b_k \beta_l^k 2^{-2k}. \quad (12)$$

$$\begin{aligned} b_0 &= 6[(48 + 24\beta_l^2 + \beta_l^4) \cos(\theta/2) + 2\beta_l^3 \{3 + 4\cos\theta\} + 24 \cos(3\theta/2) - 24\beta_l \cos(2\theta)], \\ b_1 &= 6[\beta_l(6 + \beta_l^2) - 24 \cos(\theta/2) - \beta_l(72 + \beta_l^2) \cos \theta - 8(6 + \beta_l^2) \cos(3\theta/2) + 24 \cos(5\theta/2)], \\ b_2 &= 6 \cos(\theta/2) [\beta_l^2 + 6\beta_l \cos(\theta/2) + 2 - 16 \cos \theta], \\ b_3 &= \beta_l + 4 \cos(\theta/2). \end{aligned}$$

$$\Phi_{EB3} = \frac{192[1 + 2 \cos \theta] - 192\beta_l \cos(3\theta/2) + 48\beta_l^2 [1 - 2 \cos \theta] + 16\beta_l^3 \cos(\theta/2) + \beta_l^4}{\beta_l^3 [\beta_l + 4 \cos(\theta/2)]}, \quad (13)$$

$$\Phi_{GB3} = [\beta_l^2/96 \cos \theta] \Phi_{EB3}.$$

If $\theta = \pi/2$ (this corresponds to $G \rightarrow \infty$), then applying the substitution $\beta_l = \beta_l/\sqrt{2}$ in (9), (10), (12), and (13) yields expressions for the Euler–Bernoulli approximation derived in the papers [15] and [21].

Relations (9)–(12) are valid for $k_W EI < 4G^2 A^2$ and $\theta \in (0, \pi/2]$. This requires large values of G . Considering $k_W \approx E_B$ and the beam to be cylindrical, we obtain the condition $G > \sqrt{E_B E}/16\pi$. The consistency of (9) or (13) with measurements for $\theta = 0$ violates this condition. In this case, for small values of G , relations (9)–(13) should be applied after substitution $\theta \rightarrow i \cdot \theta^*$, and the fitting parameter should be varied in the range $\theta^* \in (0, \infty)$.

3. Analysis of AFM data

The test for the suitability of the model consists of comparing the results of an analysis of bending tests for various types of objects, namely, consoles and bridges. Data were taken from AFM bending tests [15] of $\text{MgNi}_2\text{Si}_2\text{O}_5(\text{OH})_4$ phyllosilicate nanoscrolls grown by hydrothermal synthesis [22]. Nanoscrolls were deposited on a calibration grating of rectangular grooves TGZ2 (period 3 μm , groove depth 110 nm, NT-MDT SI, Russia); they formed consoles and bridges over the grooves. The bending tests were carried out in the PeakForce QNM AFM mode, FMG01 cantilevers (NT-MDT SI, Russia) were used, and the spring constant was refined using the thermal-noise–based method [23]. AFM signals of height, peak force error and deformation were recorded [14, 15, 21]. The deformation signal was corrected taking into account the contribution of methodological factors, including slipping of the AFM tip on inclined sections of the sample [8, 14, 15]. The Gwyddion 2.55 [24] program was used to process the AFM data.

Figure 3 presents test data for a console and bridge. The processing results are, respectively, as follows: $l_C = 1037$ nm, $l_B = 1463$ nm; $d_C = 80$ nm, $d_B = 66$ nm; $k_C = 0.61$ N/m, $k_B = 8.32$ N/m; $E_{C0} = 113$ GPa, $G_{C0} = 0.13$ GPa; $E_{B0} = 146$ GPa, $G_{B0} = 0.89$ GPa; $\Phi_{EC1} = 1.26$, $\Phi_{GC1} = 4.82$; $\Phi_{EB1} = 1.55$, $\Phi_{GB1} = 2.81$; $\Phi_{EC2} = 2.56$, $\Phi_{GC2} \rightarrow \infty$; $\Phi_{EB2} = 1.58$, $\Phi_{GB2} = 2.73$; $\Phi_{EC3} = 1.82$, $\Phi_{GC3} \rightarrow \infty$; $\Phi_{EB3} = 1.38$, $\Phi_{GB3} = 5.76$.

In total, AFM test data from 27 bridges and 18 consoles were processed. It is convenient to present the results on phase planes (Fig. 4).

In Fig. 4a, each studied object is characterized by a point on the phase plane: the abscissa is the value of the ratio of the squared diameter to the length of the suspended object, d^2/l , and the ordinate is the value of $k^G = k_B$ for a bridge

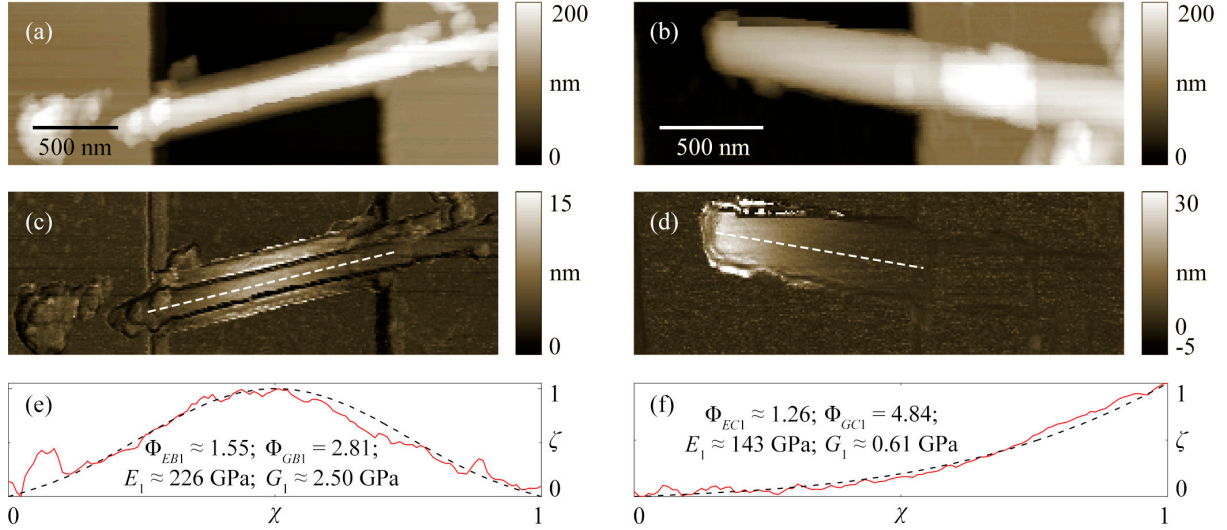


FIG. 3. AFM height images of the relief of the TGZ2 grating fragments with a recess overlapped by (a) a bridge and (b) a console of $\text{MgNi}_2\text{Si}_2\text{O}_5(\text{OH})_4$ nan scrolls. AFM maps of the corrected deformation signal of the bridge (c) and console (d). The dashed lines indicate where the deformation profiles were extracted. Normalized deformation (displacement) profiles of the bridge (e) and console (f): red solid lines — experiment, black dashed lines — approximation according to model 1. AFM imaging was performed with Peak Force Amplitude and Frequency of 150 nm and 1 kHz, respectively. The Peak Force Setpoint and the Scan Rate were as follows: 60 nN, 0.3 Hz (bridge) and 15 nN, 0.2 Hz (console).

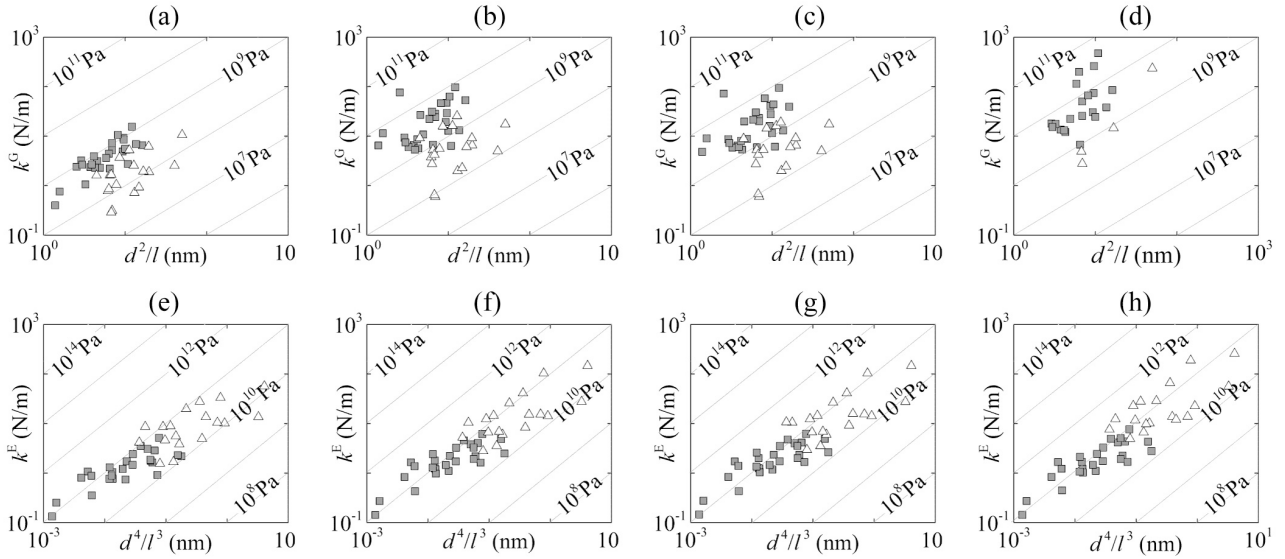


FIG. 4. Distributions of AFM bending test data for bridges (filled squares) and consoles (hollow triangles) made of $\text{MgNi}_2\text{Si}_2\text{O}_5(\text{OH})_4$ on phase planes. Calculation results: shear only (a) and bending only (e); model 1, (b) and (f); model 2, (c) and (g); model 3, (d) and (h). The inclined straight lines show the isolines of the shear modulus G in (a)—(d) and the isolines of the Young's modulus E in (e)—(h).

or $k^G = 4k_C$ for a console. On a log-log scale, according to (5a) and (5), the isolines of G are straight lines with a unit slope. The results of applying models 1–3 are depicted in Figs. 4b–4d; $k^G = \Phi_{GBj}k_B$ for a bridge and $k^G = 4\Phi_{GCj}k_C$ for a console, $j = 1-3$.

On the phase planes in the bottom row of Fig. 4, the abscissa of a point is the value of d^4/l^3 , and the ordinate is the value of $k^E = k_B$ for a bridge or $k^E = 64k_C$ for a console, Fig. 4e; in Figs. 4f–4h, the ordinate of a point is, respectively, the value of $k^E = \Phi_{EBj}k_B$ or $k^E = 64\Phi_{ECj}k_C$, $j = 1-3$. According to (5a) and (5), in this representation the isolines of E have a unit slope coefficient.

TABLE 4. Elastic moduli for $\text{MgNi}_2\text{Si}_2\text{O}_5(\text{OH})_4$. Results of using different models for processing data of AFM bending tests of a suspended object. ¹The number of test objects.

j , model no.	$G \pm \sigma(G)$ (GPa)			$E \pm \sigma(E)$ (GPa)		
	Bridge	Console	Both	Bridge	Console	Both
0	0.7 ± 0.3 (27)	0.2 ± 0.1 (18)	0.5 ± 0.3 (45)	74 ± 51 (27)	51 ± 48 (18)	66 ± 49 (45)
1	4.3 ± 5.5 (27)	0.7 ± 0.7 (18)	2.9 ± 4.6 (45)	100 ± 69 (27)	75 ± 62 (18)	90 ± 67 (45)
2	3.9 ± 5.2 (27)	0.7 ± 0.6 (17)	2.7 ± 4.4 (44)	104 ± 72 (27)	84 ± 79 (18)	96 ± 75 (45)
3	9.7 ± 11.5 (20)	1.7 ± 2.0 (4)	8.3 ± 10.9 (24)	97 ± 63 (27)	115 ± 92 (18)	103 ± 75 (45)

Since a bridge with the average span length $\langle l_B \rangle = 1.6 \pm 0.2 \mu\text{m}$ is several times longer than a console with $\langle l_C \rangle = 0.5 \pm 0.2 \mu\text{m}$, on the phase planes, data on bridges are located to the left of console data. In the zero version (Table 4), the Young's modulus of a bridge is approximately one and a half times greater than that of a console. Therefore, in Fig. 4e, the cluster of points is elongated at a flatter angle than the isolines of E . In Figs. 4f—4h, the average slope coefficients of the clusters of points become closer to unity, in accordance with the decrease in the discrepancy between the average Young's moduli of bridge and console determined from models 1–3 (Table 4). Application of model 3 produces minimal discrepancy.

In the zero version, the values of G for consoles and bridges differ several times, and the discrepancy increases after processing with the use of models 1–3. Unlike the bottom row in Fig. 4, on the phase planes of the top row, clusters of points are not aligned along isolines. This demonstrates the fact that in AFM testing, the displacement of a suspended object is controlled by bending strains rather than shear strains. In the fitting curves (Table 2 and (9) for consoles and Table 3 and (12) for bridges), the coefficients of the terms linear in χ and $\chi - \chi^2$ decrease with increasing shear modulus. For the boundary conditions of model 3, the linear terms will also be presented in shear-neglecting fitting dependences obtained in the Euler–Bernoulli approximation [15]. This is partly why the values of G determined in the Timoshenko approximation using this model are the largest in Table 4, at the level of 10 GPa. Note that the calculation of the elastic moduli of chrysotile nanoscrolls using the density functional theory (DFT) method gives shear moduli comparable to this level [14, 22]. This closeness of calculations with measurements and, at the same time, better consistency of the average values of the Young's modulus of bridges and consoles makes model 3 preferable. It remains to add that the six-fold difference in the shear moduli of bridges and consoles according to this model in Table 4 is overrated — out of eighteen consoles, fourteen consoles correspond to the case of $G \rightarrow \infty$ without participating in the statistics.

4. Conclusions

The procedure for AFM bending test of suspended rod-shaped objects has been improved. To process measurements and determine Young's and shear moduli of the material of objects, theoretical dependences of the bending of a suspended beam segment at a load point on the position of this point on the segment are obtained. Three models of boundary conditions are considered. The suitability of the models was studied by processing data from AFM bending tests of bridges and consoles made of $\text{MgNi}_2\text{Si}_2\text{O}_5(\text{OH})_4$ nanoscrolls. The minimum discrepancy between the average Young's moduli of such bridges and consoles and, at the same time, the best agreement between the experimental values of elastic moduli and the results of DFT calculations is provided by the Winkler model of a beam on an elastic foundation.

References

- [1] Binnig G., Quate C.F., Gerber Ch. Atomic Force Microscope. *Phys. Rev. Lett.*, 1986, **56**(9), P. 930–933.
- [2] Bhushan B. *Nanotribology and Nanomechanics. An Introduction*. Springer-Verlag, Berlin–Heidelberg, 2005, 928 p.
- [3] Salvétat J.-P., Kulik A. J., Bonard J.-M., Briggs G., Andrew D., Stöckli T., Méténier K., Bonnamy S., Béguin F., Burnham N. A., Forró L. Elastic Modulus of Ordered and Disordered Multiwalled Carbon Nanotubes. *Adv. Mater.*, 1986, **11**(2), P. 161–165.
- [4] Cuenot S., Demoustier-Champagne S., Nysten B. Elastic Modulus of Polypyrrole Nanotubes. *Phys. Rev. Lett.*, 1999, **85**(8), P. 1690–1693.
- [5] Kis A. Mechanical properties of mesoscopic objects. // PhD Thesis. Lausanne, 2003, 166 p.
- [6] Gangadean D., McIlroy D.N., Faulkner B.E., Aston D.E. Winkler boundary conditions for three-point bending tests on 1D nanomaterials. *Nanotechnology*, 2010, **21**(22), P. 225704.
- [7] Landau L.D., Lifshitz E.M. *Theory of Elasticity*. Pergamon Press, Oxford, 1970. 177 p.
- [8] Ankudinov A.V., Khalisov M.M. Contact Stiffness Measurements with an Atomic Force Microscope. *Tech. Phys.*, 2020, **65**(11), P. 1866–1872.
- [9] Mai W., Wang Zh.L. Quantifying the elastic deformation behavior of bridged nanobelts. *Appl. Phys. Lett.*, 2006, **89**(7), P. 073112.
- [10] Chen Yu., Dorgan B.L., McIlroy D.N., Eric Aston D. On the importance of boundary conditions on nanomechanical bending behavior and elastic modulus determination of silver nanowires. *J. Appl. Phys.*, 2006, **100**(10), P. 104301.
- [11] Kluge D., Abraham F., Schmidt S., Schmidt H.-W., Fery A. Nanomechanical Properties of Supramolecular Self-Assembled Whiskers Determined by AFM Force Mapping. *Langmuir*, 2010, **26**(5), P. 3020–3023.

- [12] Ankudinov A.V. A New Algorithm for Measuring the Young's Modulus of Suspended Nanoobjects by the Bending-Based Test Method of Atomic Force Microscopy. *Semiconductors*, 2010, **53**(14), P. 1891–1899.
- [13] Khalisov M.M., Lebedev V.A., Poluboyarinov A.S., Garshev A.V., Khrapova E.K., Krasilin A.A., Ankudinov A.V. Young's modulus of phyllosilicate nanoscrolls measured by the AFM and by the in-situ TEM indentation. *Nanosyst.: Phys. Chem. Math.*, 2021, **12**(1), P. 118–127.
- [14] Krasilin A.A., Khalisov M.M., Khrapova E.K., Kunkel T.S., Kozlov D.A., Anuchin N.M., Enyashin A.N., Ankudinov A.V. Surface Tension and Shear Strain Contributions to the Mechanical Behavior of Individual Mg-Ni-Phyllosilicate Nanoscrolls. *Part. Part. Syst. Charact.*, 2021, **38**(12), P. 2100153.
- [15] Ankudinov A., Dunaevskiy M., Khalisov M., Khrapova E., Krasilin A. Atomic force microscopy bending tests of a suspended rod-shaped object: Accounting for object fixing conditions. *Phys. Rev. E.*, 2021, **107**(2), P. 025005.
- [16] Winkler E. *Die Lehre von der Elastizität und Festigkeit*. Dominicus, Prague, 1867, 388 p.
- [17] Lekhnitskii S.G. *Theory of Elasticity of an Anisotropic Body*. Holden-Day, San Francisco, 1963, 404 p.
- [18] Ting T.C.T., Chen T. Poisson's ratio for anisotropic elastic materials can have no bounds. *Q. J. Mech. Appl. Math.*, 2005, **58**(1), P. 73–82.
- [19] Timoshenko S.P. On the correction for shear of the differential equation for transverse vibrations of prismatic bars. *London Edinburgh Dublin Philos. Mag. J. Sci.*, 1921, **41**(245), P. 744–746.
- [20] Cowper G.R. The Shear Coefficient in Timoshenko's Beam Theory. *J. Appl. Mech.*, 1966, **33**(2), P. 335–340.
- [21] Ankudinov A.V., Khalisov M.M. Bending test of nanoscale consoles in atomic force microscope. *Tech. Phys. Lett.*, 2022, **48**(2), P. 21–24.
- [22] Khrapova E.K., Ugolkov V.L., Straumal E.A., Lermontov S.A., Lebedev V.A., Kozlov D.A., Kunkel T.S., Nominé A., Bruyere S., Ghanbaja J., Belmonte T., Krasilin A.A. Thermal behavior of Mg-Ni-phyllosilicate nanoscrolls and performance of the resulting composites in hexene-1 and acetone hydrogenation. *ChemNanoMat*, 2021, **7**(3), P. 207–207.
- [23] Hutter J.L., Bechhoefer J. Calibration of atomic-force microscope tips. *Rev. Sci. Instrum.*, 1993, **64**(7), P. 1868–1873.
- [24] Nečas D., Klapetek P. Gwyddion: an open-source software for SPM data analysis. *Open Phys.*, 2012, **10**(1), P. 181–188.

Submitted 24 November 2023; accepted 12 February 2024

Information about the authors:

Alexander V. Ankudinov – Ioffe Institute, Polytekhnicheskaya, 26, St. Petersburg, 194021, Russia; ORCID 0000-0002-3450-0420; alexander.ankudinov@mail.ioffe.ru

Mikhail S. Dunaevskiy – Ioffe Institute, Polytekhnicheskaya, 26, St. Petersburg, 194021, Russia; ORCID 0000-0001-6038-223X; mike.dunaeffsky@mail.ioffe.ru

Andrei A. Krasilin – Ioffe Institute, Polytekhnicheskaya, 26, St. Petersburg, 194021, Russia; ORCID 0000-0002-3938-3024; ikrasilin@mail.ioffe.ru

Maksim M. Khalisov – Ioffe Institute, Polytekhnicheskaya, 26, St. Petersburg, 194021, Russia; Pavlov Institute of Physiology, Russian Academy of Sciences, Makarova emb., 6, St. Petersburg, 199034, Russia; ORCID 0000-0002-5171-4690; khalisovmm@infran.ru

Ekaterina K. Khrapova – Ioffe Institute, Polytekhnicheskaya, 26, St. Petersburg, 194021, Russia; ORCID 0000-0003-2674-9653; arganella@yandex.ru

Conflict of interest: the authors declare no conflict of interest.